Available online at www.sciencedirect.com
ScienceDirect
Journal of Magnetic Resonance 188 (2007) 49–55
JMR Journal of Magnetic Resonance
www.elsevier.com/locate/jmr

Using chemical shift anisotropy to resolve isotropic signals in solid-state NMR

Matthew S. Ironside, Robin S. Stein, Melinda J. Duer *

University Chemical Laboratories, Lensfield Road, Cambridge CB2 1EW, UK

Received 27 March 2007; revised 6 June 2007
Available online 15 June 2007

Abstract

A key problem in solid-state NMR is resolving overlapping isotropic signals. We present here a two-dimensional method which can enable sites with the same isotropic chemical shift to be distinguished according to their chemical shift anisotropy and asymmetry. The method involves correlating sideband spectra at different effective spinning rates using CSA-amplification pulse sequences. The resulting two-dimensional correlation pattern allows very accurate determination of the chemical shift principal values in addition to the recovery of parameters for two overlapping patterns which allows the resolution of overlapping signals.

Keywords: CSA recoupling; CSA-amplified PASS; Overlapping signals; Spinning sidebands; ^{31}P NMR

1. Introduction

The chemical shift [1] is the most widely used property of NMR spectroscopy. Its strong dependence on the environment of the nucleus means that it can be used to investigate structure and chemistry to great effect [2].

A longstanding problem in NMR has been how to deal with the case where two sites yield the same isotropic chemical shift and so have overlapping signals in the NMR spectrum. In favourable cases, signals may be resolved in an appropriate multi-dimensional spectrum where peaks are correlated via dipolar or *J*-coupling. However, for an isolated spin system, or one where the only possible nucleus for correlation is one which itself gives poor spectral resolution, methods for resolving signals are lacking. This situation arises frequently for natural abundance ^{13}C and ^{15}N spectra of organic species, for instance.

The chemical shift arises from a second-rank tensorial property, the chemical shielding [3]. Two sites with the same isotropic chemical shift do not necessarily have the same associated shielding tensors. On the contrary, the individual principal values of the shielding tensors may be quite different, and this gives us the possibility of resolving two signals via the chemical shift anisotropy and asymmetry, rather than the more usual isotropic chemical shift. This work presents a methodology by which this may be achieved in practice.

The methodology utilises one of the recently developed two-dimensional isotropic–anisotropic correlation methods for measuring the chemical shift anisotropy. In such techniques, an isotropic chemical shift dimension is correlated with a pattern in the second spectral dimension that represents the chemical shift anisotropy (CSA) [4,5]. These methods fall into two broad groups, with the chemical shift anisotropy pattern being represented by (i) spinning sideband patterns [6–13] or (ii) powder patterns [14–19].

In the vast majority of cases, the isotropic spectral dimension is generated by rapid magic-angle spinning (MAS). Consider instead the case where such an experiment is performed at a spinning rate that is slow compared to the chemical shift anisotropies being measured. The isotropic spectral dimension then consists of a spinning sideband pattern, and the two-dimensional plane correlates

* Corresponding author.
E-mail address: mjd13@cam.ac.uk (M.J. Duer).

1090-7807/$ - see front matter © 2007 Elsevier Inc. All rights reserved.
doi:10.1016/j.jmr.2007.06.003

two sideband patterns in the case of experiments falling into category (i) or a sideband pattern with a powder pattern for those in category (ii).

Such a two-dimensional chemical shift sideband–sideband or sideband–powder pattern correlation spectrum resolves more information about overlapping signals than a one-dimensional sideband or powder pattern. Consider the extreme case of two overlapping patterns with the same isotropic shift, where one arises from a much larger chemical shift anisotropy than the other. This is illustrated in Fig. 1 for the case of sidebands (in the direct dimension) correlated with sidebands (in the indirect dimension). In the two-dimensional correlation pattern, the outermost sidebands in the direct (ω_2) dimension contain mostly signal from the larger CSA component. Thus the spinning sideband or powder patterns correlated with these outermost sidebands may be readily analysed to yield the chemical shift parameters for this component alone. The lower order sidebands in the direct dimension will contain signal from both components, but sideband or powder patterns correlated with these sidebands may now be easily analysed to reveal the chemical shift parameters of the smaller CSA component, as those for the other component are already known. In this way, the chemical shift parameters of the two components may be uniquely determined.

In the more general case, where the chemical shift parameters of the two components are similar, there is still the possibility of determining parameters for both components. For each sideband in the direct dimension, there is a correlated spinning sideband or powder pattern which is a sum of the patterns associated with the two sites. The ratio of the intensities of each component within each sideband or powder pattern is determined by (a) the relative populations of the two sites and (b) the relative sizes of their respective chemical shift anisotropies. Hence, unless the two sets of chemical shift parameters give spinning sideband or powder patterns which are indistinguishable within the level of noise, one can in principle uniquely determine them from the two-dimensional correlation pattern, something which has been shown to be extremely difficult when using a one-dimensional sideband pattern and possible only some of the time when using a one-dimensional powder pattern [20].

We concentrate here on the correlation of two spinning sideband patterns to resolve overlapping isotropic signals, for in general one can expect a better signal-to-noise ratio from such an experiment. However, the case of correlating sideband patterns and powder patterns also has its merits and will be considered in a later paper. To correlate two spinning sideband patterns, we simply require a two-dimensional experiment in which the effective spinning rate in the indirect dimension is different to that in the direct dimension. One group of experiments which fulfil this requirement are those based on the 2D-PASS experiment [21] of Antzutkin et al., although the 2D-PASS experiment itself does not scale the spinning rate. These experiments employ a series of radiofrequency pulses applied in a fixed, rotor-synchronised time interval to recouple the anisotropic part of the chemical shielding. The advantage of these types of experiment is that relatively few increments are required in the indirect time dimension. A number of such experiments are known [8,11–13]; in this work, we

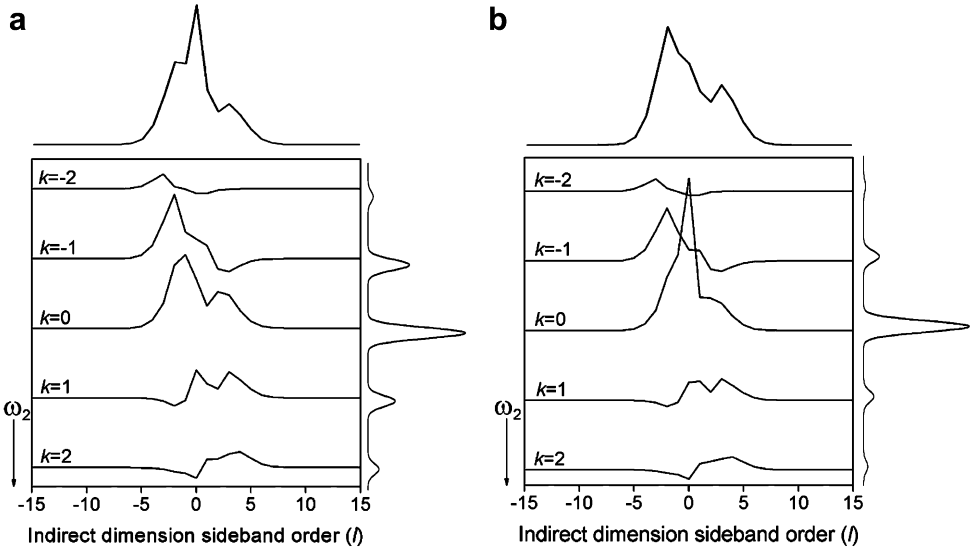

Fig. 1. (a) A simulated two-dimensional sideband correlation pattern from a CSA-amplified PASS experiment [12] for a component with $\Delta = 6000$ Hz and $\eta = 0.5$, with the spinning rate, $\omega_r = 3$ kHz, and effective spinning rate in the indirectly observed dimension, $\omega_r/N = 1$ kHz. Slices showing the spinning sideband intensity envelope are correlated with the sidebands in the higher spinning rate (directly observed, ω_2) dimension, with sideband order, k. Projections onto both the spectral axes are also shown. (b) A simulated two-dimensional sideband correlation pattern from a CSA-amplified PASS experiment for the same component with $\Delta = 6000$ Hz and $\eta = 0.5$, overlapped with a component with $\Delta = 1000$ Hz and $\eta = 0.8$ in equal proportions. The effect of the second component can only be seen in the $k = 0$ direct dimension sideband, so the other sidebands can be used reliably to determine parameters for the $\Delta = 6000$ Hz component.

use the CSA-amplified PASS experiment [12], in which the pulse sequence effectively scales the spinning rate in the indirect spectrum by a factor of N.

Crockford et at. [8] have shown the signal, $s_c(\Theta, t_2)$, from such an experiment is described by

$$s_c(\Theta,t_2)=\sum_{l'}\sum_{l}\sum_{k}F_c^{(l')}\left[C_c^{(k+l'-l)}\right]^*[F_c^{(l)}]^*C_c^{(k)} \times \exp(i((\omega_{iso}+k\omega_r)t_2+l\Theta)), \quad (1)$$

where Θ is a dummy t_1 variable that is incremented between 0 and 2π, ω_r is the sample spinning rate, the subscript c denotes a carousel [22] and $F_c^{(l)}$ and $C_c^{(k)}$ are complex Fourier components that are defined in the reference. The intensity of the two-dimensional peak with sideband order k in the direct dimension and l in the indirect dimension can be shown to be [8]

$$a_c^{(k,l)}=\sum_{l'}F_c^{(l')}\left[C_c^{(k+l'-l)}\right]^*[F_c^{(l)}]^*C_c^{(k)}. \quad (2)$$

In a one-dimensional spectrum, the sideband intensities can be shown to be

$$a_c^{(l)}=F_c^{(l)}F_c^{(l)*}. \quad (3)$$

Thus the one-dimensional pattern depends on the squared modulus of the Fourier components, $F_c^{(l)}$, whilst the two-dimensional sideband correlation pattern, described by Eq. (2), is determined by $F_c^{(l)}$ and $C_c^{(k)}$ and so retains information about the phases of these terms as well as their magnitude. Thus the two-dimensional correlation pattern has a fundamentally greater information content than a one-dimensional pattern and should allow more accurate determination of the chemical shift parameters. This is especially important when using a least-squares fitting procedure to derive the chemical shift parameters from the sideband patterns, as altering the chemical shift parameters from their best fit causes a greater change in the form of the spectrum and so a higher sum of squared error than the change when fitting a one-dimensional spectrum.

The idea of correlating chemical shift spectra obtained under different chemical shift anisotropy recoupling conditions is not in itself new. Nishiyama et al. [23] correlated off-magic-angle spinning (OMAS) powder patterns with powder patterns obtained from recoupling just the part of the chemical shift hamiltonian that depends on $2\omega_r t$. This results in a two-dimensional correlation pattern which may be analysed to reveal the principal values of the chemical shift tensor very accurately. The only problem with this method is that it relies on spinning the sample away from the magic angle and, therefore, resolution is severely compromised, both as a result of the presence of chemical shift anisotropy powder patterns appearing in both spectral dimensions and as a result of residual dipolar coupling broadening the spectra.

An alternative method has also been proposed for separating signals according to chemical shift anisotropy and asymmetry by de Swiet [24,25], via an ingenious transform of a two-dimensional time domain dataset in which different spherical tensor components of the shielding tensor are recoupled in each domain. The result of the transform is a spectrum of (in effect) the chemical shift anisotropies and asymmetries in the sample. This would be an ideal solution to the problem of overlapping isotropic signals in the frequency domain, but the author cautions that further work is needed before this method could be generally applicable. In particular, pulse imperfections lead to significant errors in the chemical shift anisotropies determined and so far has not been pursued further.

Our methodology is demonstrated here for ^{31}P CSA-amplified PASS on a mixture of hydroxyapatite, $Ca_{10}(PO_4)_6(OH)_2$ and sodium dihydrogen phosphate, $NaH_2PO_4{\cdot}H_2O$, for which the phosphate sites show very similar ^{31}P isotropic shifts.

2. Results and discussion

2.1. Simulations

Simulations were used first to determine the optimum correlated spinning rates for extracting accurate values for the anisotropies in the case of well-resolved signals, where the spinning sideband pattern corresponds to a single chemical site. Spectra were generated for a signal with a particular value of Δ, and $\eta = 0.5$, using Eq. (2), for various pairs of correlated spinning rates, ω_r, and ω_r/N. Percentage errors in fits of Δ and η were estimated using the Cramér–Rao lower bounds method [26,27]. Results are shown in Fig. 2.

The lowest errors in Δ occur for the special case of $N = 1$, with $\omega_r = \omega_r/N = 0.4\Delta$, the condition for the 2D-PASS experiment (i.e. a one-dimensional sideband pattern with five visible sidebands). This is expected as the signal intensity is concentrated into only five peaks and so is less affected by noise [20]. However, in general there will be more than one chemical site in a molecule and a single spinning rate cannot minimise errors in Δ for all chemical sites. Fig. 2 shows clearly that for CSA-amplified PASS with, say, $N = 2$, there is a wider range of spinning rates that allow determination of Δ with errors not much greater than the lowest possible errors. On the other hand, for $N = 1$ (i.e. 2D-PASS), the errors increase relatively rapidly away from the $\omega_r = 0.4\Delta$ condition. This is equivalent to saying that for a particular experiment, with given ω_r and $N > 1$, there is a wider range of Δ that can be determined with reasonable accuracy than with 2D-PASS. Errors in η are similar in both $N = 1$ and $N \neq 1$ cases.

It is useful to compare the relative errors arising from fitting one- and two-dimensional sideband pattern datasets. A one-dimensional sideband pattern is equivalent to a projection of a CSA-amplified PASS experiment taken onto one of the axes of the two-dimensional spectrum. If this is done, the net signal intensity decreases because the two-dimensional correlation pattern has both positive and negative components and so there is some cancellation

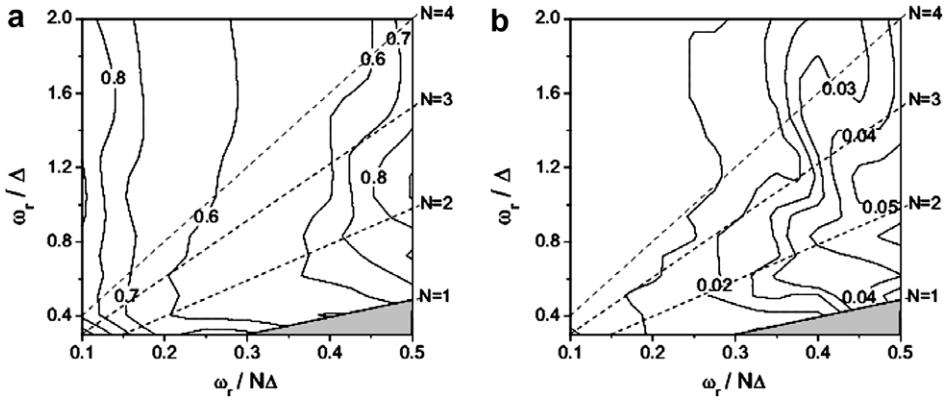

Fig. 2. Contour plots showing the percentage error in the best fit of (a) Δ and (b) η from least-squares fitting of a single-component two-dimensional simulated spectrum with correlated spinning rates ω_r and ω_r/N in the direct and indirect dimensions, respectively, with random noise added as described in Section 4. The diagonal lines join points corresponding to experiments with equal scaling factor, N, and the grey region indicates the unachievable situation of $N < 1$.

of signal in the formation of the projection. Thus, the signal-to-noise ratio in the one-dimensional projected spectrum (i.e. a one-dimensional sideband pattern) is less than that in the two-dimensional correlation pattern and the accuracy of a fit from a projection is correspondingly decreased. Analysis of these projections show that the chemical shift anisotropy is determined most accurately, as expected, when $\omega_r = 0.4\Delta$, irrespective of the value of ω_r. If a two-dimensional correlation pattern is recorded with $\omega_r/N = 0.4\Delta$ and fitted instead, the resulting errors are just over half of those found from fitting the one-dimensional dataset for the same noise level per data point prior to projection. Even lower errors result if, rather than choosing $\omega_r/N = 0.4\Delta$, ω_r and ω_r/N in the two-dimensional experiment are chosen to be in the lowest error regions of Fig. 2. This means that using two-dimensional sideband correlation patterns, rather than projections, has merit even for determining Δ for well-resolved signals.

Simulations were then performed to determine the optimum values of ω_r and ω_r/N for overlapping signals. Five variables must be considered when fitting two overlapping spinning sideband patterns: the anisotropies (Δ_1 and Δ_2) and asymmetries (η_1 and η_2) for each pattern, and the ratio of the intensities of the components. The most important conclusions from these simulations are presented in Figs. 3 and 4 and summarized below.

The optimal choice of ω_r and ω_r/N varies with the ratio of the anisotropies, Δ_1/Δ_2 (where $\Delta_1 < \Delta_2$) and must be chosen especially carefully when $\Delta_1 \approx \Delta_2$. Fig. 3 shows that errors in fitting are almost independent of ω_r (provided that ω_r is such that there are at least first order sidebands in the direct dimension), but have a strong dependence on ω_r/N. Figs. 3 and 4 also show that with fixed Δ_2, as Δ_1 is increased towards Δ_2 (i.e. the ratio Δ_1/Δ_2 approaches unity), the optimum reduced spinning rate, ω_r/N, decreases, contrary to the case where well-resolved signals are being analysed.

One final point which should be made is that the reliability of fitted parameters depends on the relative intensities of the overlapping components and the relative size of

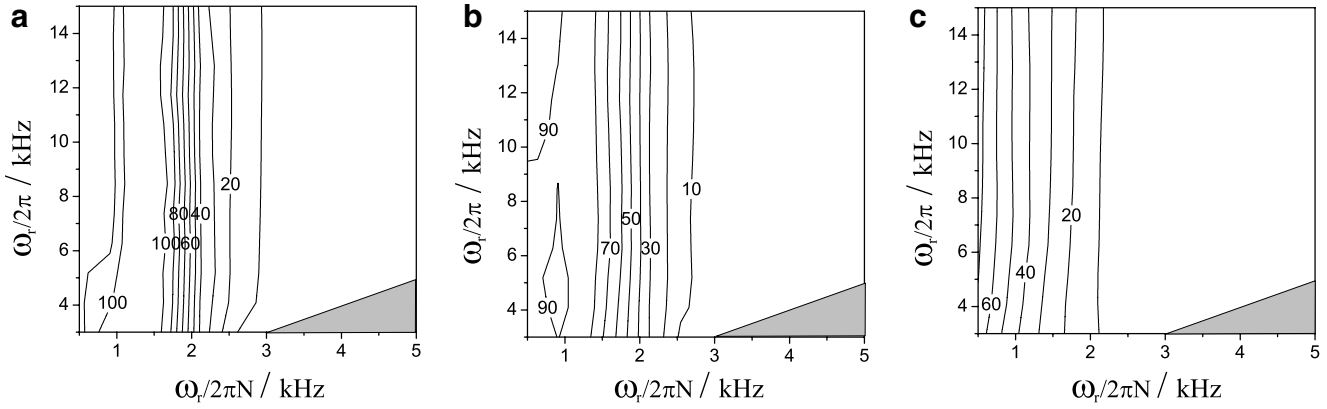

Fig. 3. Contour plots for the situation where there are two overlapping signals in equal proportions showing the dependence of the reliability (which is inversely proportional to percentage error) of the least accurate anisotropy, Δ_1 or Δ_2, on the actual spinning rate, ω_r, and reduced spinning rate ω_r/N. In each instance the larger anisotropy takes the value $\Delta_2 = 10{,}000$ Hz, with $\eta_2 = 0.5$. Δ_1 takes values of (a) 4000 Hz, (b) 6000 Hz and (c) 8000 Hz, with $\eta_1 = 0.8$. Random noise is included as described in Section 4.

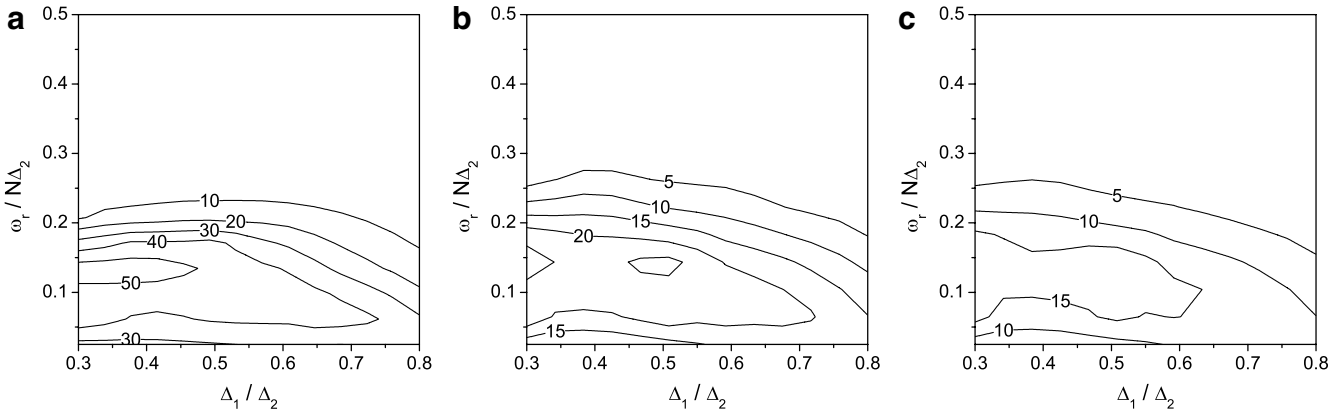

Fig. 4. Contour plots for the situation where there are two overlapping signals in unequal proportions showing the dependence of the reliability (which is inversely proportional to percentage error) of the least accurate anisotropy, Δ_1 or Δ_2, on the ratio of Δ_1/Δ_2 and the reduced spinning rate, ω_r/N. The actual spinning rate is $\omega_r = 6$ kHz and the larger anisotropy takes the value $\Delta_2 = 10{,}000$ Hz. The ratios of the two components are (a) 1:1, (b) 1:3 and (c) 1:5. Random noise is added as described in Section 4.

the chemical shift anisotropies involved, as shown in Fig. 4. To summarise the effect here, we note that the method is capable of accurately determining chemical shift parameters for overlapping components with $\Delta_1/\Delta_2 = 0.7$, where one component comprises 25% of the total signal (Fig. 4b), and components with $\Delta_1/\Delta_2 = 0.5$, with one component comprising just 15% of the total signal (Fig. 4c).

2.2. Mixtures of phosphates

The two phosphates compounds chosen, hydroxyapatite and sodium dihydrogen phosphate have isotropic shifts of around 2 ppm. The shifts are sufficiently close that with natural line broadening they appear as one peak in an isotropic spectrum, and so, since their chemical shift parameters can be determined independently, provide an excellent opportunity to demonstrate the method experimentally. The parameters determined from one- and two-dimensional sideband intensity patterns of pure compounds are given in Table 1, along with Cramér–Rao lower bounds error estimates [26,27] (note that these errors only take into account random errors—systematic errors will also be present and in general will increase with scaling factor, N). Additionally, as an example, the best fit solution for sodium dihydrogen phosphate is shown in Fig. 5.

Table 1
Best fit chemical shift parameters for resolved ^{31}P sites in hydroxyapatite and sodium dihydrogen phosphate

	Fitted parameters (1D fit)	Fitted parameters (2D fit)
Hydroxyapatite	$\Delta = 10.9 \pm 0.3$ ppm $\eta = 0.92 \pm 0.05$	$\Delta = 11.1 \pm 0.2$ ppm $\eta = 0.89 \pm 0.03$
Sodium dihydrogen phosphate	$\Delta = -80.0 \pm 0.4$ ppm $\eta = 0.468 \pm 0.004$	$\Delta = -79.6 \pm 0.2$ ppm $\eta = 0.468 \pm 0.002$

The methods used to determine them are described in Section 4. Errors are Cramér–Rao lower bounds estimates of random error. For hydroxyapatite, three sidebands are used from the direct dimension and for sodium dihydrogen phosphate, nine sidebands are used.

The two phosphates are found to have greatly different chemical shift anisotropies. Four mechanical mixtures of the two phosphates were studied (with molar phosphate ratios of 1:8, 1:1, 2:1 and 7:1 hydroxyapatite to sodium dihydrogen phosphate) and the chemical shift parameters of each component were calculated from the resulting overlapping sideband pattern using the two-dimensional approach; the results are given in Table 2. The fitted intensity ratio is not equal to the molar ratio due to differences in the cross-polarisation efficiency. The results show that, for an equal molar ratio mixture, this approach can determine values for chemical shift parameters that match well with those determined by analysis of the patterns for the separate components, even though in these proportions, the hydroxyapatite signal comprises barely 10% of the total signal (the sign error on Δ_1 results from η_1 being close to unity). As expected, the error estimates for a particular component increase as the proportion of that component in the mixture decreases. Thus no reliable fit could be found with more than 50% sodium dihydrogen phosphate by mole of phosphate units, since the hydroxyapatite comprised a too small proportion of the total signal (i.e. less than 10%).

A key issue is whether this method can be used to determine the number of components that a sideband pattern or signal comprises, or whether one must have prior knowledge of the number of components before a sensible analysis can be made. Clearly, the former feature would be highly desirable. The best fit procedure can be repeated without prior knowledge of how many components are present and assessing the χ^2 parameter arising from the fit. Obviously fitting extra parameters can always lower χ^2, so by increasing the number of components assumed to make up the signal, χ^2 will always decrease. However, when the sideband pattern arises from only one component, χ^2 is reduced by an average of 60% when attempting to fit two components to the data. However, when there are

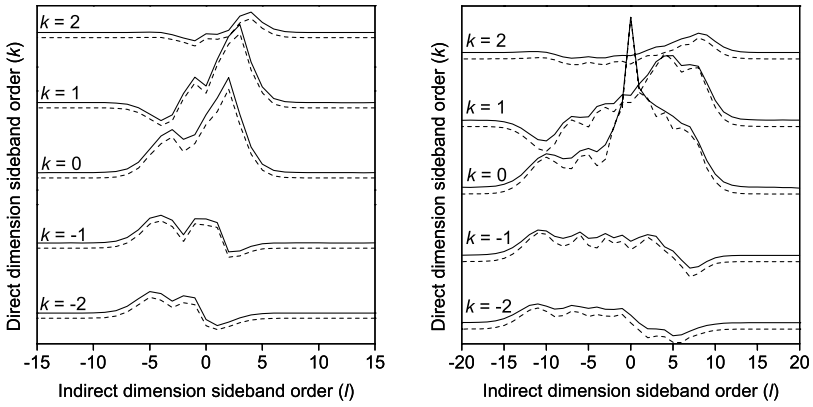

Fig. 5. Experimental ^{31}P CSA-amplified PASS sideband pattern (solid line) of sodium dihydrogen phosphate (left) with spinning rate, $\omega_r = 6$ kHz, and $N = 3.4$ giving a reduced spinning rate of $\omega_r/N = 1765$ Hz, displayed in the same manner as Fig. 1. The simulated two-dimensional sideband intensity pattern (dashed lines) using the best fit chemical shift parameters found in Table 1 is overlaid. Experimental ^{31}P CSA-amplified PASS sideband pattern (solid line) of a 1:1 mixture (by moles of phosphate) of sodium dihydrogen phosphate and hydroxyapatite (right) with spinning rate, $\omega_r = 6$ kHz, and $N = 6.8$ giving a reduced spinning rate of $\omega_r/N = 882$ Hz. The simulated two-dimensional sideband intensity pattern (dashed lines) using the best fit chemical shift parameters found in Table 2 is overlaid. For clarity, only five sidebands in the direct dimension are shown on both plots, although seven were used in the fitting.

Table 2
Best fit chemical shift parameters for ^{31}P sites for the hydroxyapatite and sodium dihydrogen phosphate mixtures described in the text, with different molar ratios of phosphate

Molar ratio	Δ_1/ppm	η_1	Δ_2/ppm	η_2	Intensity ratio
1:8	No fit located				
1:1	-11.1 ± 0.2	0.93 ± 0.04	-79.6 ± 0.2	0.453 ± 0.003	1:7.7
2:1	10.8 ± 0.2	0.96 ± 0.02	-78.8 ± 0.2	0.461 ± 0.005	1:2.6
7:1	10.4 ± 0.2	0.85 ± 0.03	-78.8 ± 0.6	0.469 ± 0.012	1:1.3

The best fits are found using the two-dimensional analysis. Δ_1 and η_1 refer to hydroxyapatite and Δ_2 and η_2 to sodium dihydrogen phosphate. The fitted intensity ratios of hydroxyapatite to sodium dihydrogen phosphate are also listed. Errors are Cramér–Rao lower bounds estimates of random error. In each case seven direct dimension sidebands were used for fitting.

actually two components present, χ^2 is reduced by over 95% in each case relative to attempting to fit only one component to the data. Thus by examining χ^2 for attempted fits with different numbers of components, one can correctly determine the number of overlapping components in the signal.

3. Conclusions

Analysing two-dimensional spinning sideband patterns arising from different (effective) spinning rates leads to significantly greater accuracy in determining the underlying chemical shift anisotropy and asymmetry compared with traditional one-dimensional methods [4,28]. Errors in the estimates of the chemical shift parameters found by least-squares analysis are approximately half those from one-dimensional methods for the same signal-to-noise ratio in the isotropic spectrum.

Moreover, this work shows that there is scope for obtaining chemical shift parameters from overlapping sideband patterns, a problem that has proven difficult to solve in the past [20]. The two-dimensional experiment discussed here provides the possibility for determining such parameters, thereby *resolving* overlapping isotropic signals. The experiment is of the kind commonly used to resolve one-dimensional spinning sidebands patterns and is straightforward to implement.

4. Experimental

Hydroxyapatite and sodium dihydrogen phosphate monohydrate were purchased from Sigma and used without further purification or recrystallisation. Experiments were performed on a Bruker Avance 400 spectrometer, operating at a phosphorus frequency of 161.9 MHz, using a double resonance 4 mm MAS probe.

The ^{31}P CSA-amplified PASS spectra were recorded of both the raw materials and mixtures in molar ratios of phosphate (of hydroxyapatite to sodium dihydrogen phosphate) of 1:8, 1:1, 2:1 and 7:1. For the all spectra, an actual spinning rate of 6 kHz was used. For the spectrum of pure hydroxyapatite, the scaling factor used was $N = 6.8$, giving a reduced spinning rate of 882 Hz, recording 32 t_1 points with 52 acquisitions per point using a cogwheel phase cycling scheme [29]. For the spectrum of pure sodium dihydrogen phosphate, the scaling factor used was $N = 3.4$, giving a reduced spinning rate of 1765 Hz, recording 32 t_1 points with 28 acquisitions per point. For the spectrum of

the mixtures, the scaling factor used was $N = 6.8$, giving a reduced spinning rate of 882 Hz, recording 44 t_1 points with 52 acquisitions per point. The recycle delay was 5 s. The ^{1}H–^{31}P cross-polarisation contact time was 8 ms. High-power TPPM proton decoupling [30] was applied with a field strength of 78 kHz. The two-dimensional sideband intensity patterns used for fitting were generated by integrating the slices in the indirect dimension over the sideband peak-width in the direct dimension. The CSA-amplified PASS experiment results in net sideband intensities in the f_1 dimension of the 2D experiment, so no further processing is required to extract the sideband intensities in f_1. The one-dimensional sideband patterns were calculated by summing intensities over all visible sidebands in the f_2 dimension of the above experiment, giving a projected sideband pattern corresponding to the reduced spinning rate, ω_r/N.

Numerical simulations of two-dimensional sideband spectra were performed using a procedure written in the PV-Wave environment [31]. Eq. (2) was evaluated and summed for 233 α and β angles generated by a REPULSION algorithm [32]. Best fits were found using a least-squares fitting routine to minimise χ^2. Initial estimates of chemical shielding parameters were generated randomly within usual ranges of these parameters for ^{31}P. For fitting of simulated spectra, random noise was generated with a standard deviation of 1/300 of the total signal intensity under all of the sidebands, and added to the simulated spectrum prior to fitting. As many sidebands in f_2 were used as were visible above the noise level, and all f_1 points were used in the fits.

Acknowledgments

We are grateful to the Engineering and Physical Sciences Research Council for a studentships (M.S.I.) and a Gates Foundation studentship (R.S.S.). We also acknowledge Robin Orr for useful discussion.

References

[1] W.G. Proctor, F.C. Yu, The dependence of a nuclear magnetic resonance frequency upon chemical compound, Phys. Rev. 77 (1950) 717.
[2] N.F. Ramsey, Magnetic shielding of nuclei in molecules, Phys. Rev. 78 (1950) 699–703.
[3] M. Mehring, Principles of High Resolution NMR in Solids, Second ed., Springer-Verlag, Berlin, Germany, 1983.
[4] M.M. Maricq, J.S. Waugh, NMR in rotating solids, J. Chem. Phys. 70 (1979) 3300–3316.
[5] N. Bloembergen, T.J. Rowland, On nuclear magnetic resonance in metals and alloys, Acta Metall. 1 (1953) 731–746.
[6] T. Gullion, Extended chemical shift modulation, J. Magn. Reson. 85 (1989) 614–619.
[7] A.C. Kolbert, R.G. Griffin, Two-dimensional resolution of isotropic and anisotropic chemical-shifts in magic-angle spinning NMR, Chem. Phys. Lett. 166 (1990) 87–91.
[8] C. Crockford, H. Geen, J.J. Titman, Two-dimensional MAS-NMR spectra which correlate fast and slow magic angle spinning sideband patterns, Chem. Phys. Lett. 344 (2001) 367–373.
[9] B. Eléna, S. Hediger, L. Emsley, Correlation of fast and slow chemical shift spinning sidebands under fast magic-angle spinning, J. Magn. Reson. 160 (2003) 40–46.
[10] M. Strohmeier, D.M. Grant, A new sensitive isotropic–anisotropic separation experiment—SPEED MAS, J. Magn. Reson. 168 (2004) 296–307.
[11] L.M. Shao, C. Crockford, H. Geen, G. Grasso, J.J. Titman, Chemical shift anisotropy amplification, J. Magn. Reson. 167 (2004) 75–86.
[12] R.M. Orr, M.J. Duer, S.E. Ashbrook, Correlating fast and slow chemical shift spinning sideband patterns in solid-state NMR, J. Magn. Reson. 174 (2005) 301–309.
[13] L. Shao, C. Crockford, J.J. Titman, Chemical shift anisotropy amplification with high amplification factor and improved sensitivity, J. Magn. Reson. 178 (2006) 155–161.
[14] Z. Gan, High-resolution chemical shift and chemical shift anisotropy correlation in solids using slow magic angle spinning, J. Am. Chem. Soc. 114 (1992) 8307–8310.
[15] L. Frydman, G. Chingas, Y. Lee, P. Grandinetti, M. Eastman, G. Barrall, A. Pines, Variable-angle correlation spectroscopy in solid-state nuclear magnetic resonance, J. Chem. Phys. 97 (1992) 4800–4808.
[16] R. Tycko, G. Dabbagh, P.A. Mirau, Determination of chemical-shift-anisotropy lineshapes in a two-dimensional magic-angle-spinning NMR experiment, J. Magn. Reson. 85 (1989) 265–274.
[17] S.F. Liu, J.D. Mao, K. Schmidt-Rohr, A robust technique for two-dimensional separation of undistorted chemical-shift anisotropy powder patterns in magic-angle-spinning NMR, J. Magn. Reson. 155 (2002) 15–28.
[18] J.C.C. Chan, R. Tycko, Recoupling of chemical shift anisotropies in solid-state NMR under high-speed magic-angle spinning and in uniformly ^{13}C-labelled systems, J. Chem. Phys. 118 (2003) 8378–8389.
[19] R.M. Orr, M.J. Duer, Recoupling of chemical shift anisotropy powder patterns in MAS-NMR, J. Magn. Reson. 181 (2006) 1–8.
[20] P. Hodgkinson, L. Emsley, The reliability of the determination of tensor parameters by solid-state nuclear magnetic resonance, J. Chem. Phys. 107 (1997) 4808–4816.
[21] O.N. Antzutkin, S.C. Shekar, M.H. Levitt, Two-dimensional sideband separation in magic-angle-spinning NMR, J. Magn. Reson. A 115 (1995) 7–19.
[22] M.H. Levitt, Why do spinning sidebands have the same phase? J. Magn. Reson. 82 (1989) 427–433.
[23] Y. Nishiyama, T. Yamazaki, T. Terao, Development of modulated rf sequences for decoupling and recoupling of nuclear-spin interactions in sample-spinning solid-state NMR: application to chemical-shift anisotropy determination, J. Chem. Phys. 124 (2006) 064304.
[24] T.M. de Swiet, A direct transform for the nuclear magnetic resonance chemical shift anisotropy, J. Chem. Phys. 110 (1999) 5231–5237.
[25] T.M. de Swiet, Three-dimensional measurements of the nuclear magnetic resonance chemical shift and a new analytic data transform for the shift anisotropy, J. Chem. Phys. 112 (2000) 8567–8572.
[26] W.E. Wentworth, Rigorous least squares adjustment: application to some non-linear equations, J. Chem. Ed. 42 (1965) 96–103.
[27] A.C. Olivieri, Rigorous statistical analysis of errors in chemical-shift-tensor components obtained from spinning sidebands in solid-state NMR, J. Magn. Reson. A 123 (1996) 207–210.
[28] J. Herzfeld, A.E. Berger, Sideband intensities in NMR spectra of samples spinning at the magic angle, J. Chem. Phys. 73 (1980) 6021–6030.
[29] M.H. Levitt, P.K. Madhu, C.E. Hughes, Cogwheel phase cycling, J. Magn. Reson. 155 (2002) 300–306.
[30] A.E. Bennet, C.M. Rienstra, M. Auger, K.V. Lakshmi, Heteronuclear decoupling in rotating solids, J. Chem. Phys. 103 (1995) 6951–6958.
[31] Visual Numerics, PV-Wave Advantage, computer program, 1993.
[32] M. Bak, N.C. Nielsen, REPULSION: a novel approach to efficient powder averaging in solid-state NMR, J. Magn. Reson. 125 (1997) 132–139.